

Formation of lead halide perovskite precursors in solution: Insight from electronic-structure theory

Richard Schier,¹ Alejandro Conesa Rodriguez,¹ Ana M. Valencia,^{1,2} and Caterina Cocchi^{1,2}

¹Humboldt-Universität zu Berlin, Physics Department and IRIS Adlershof, 12489 Berlin, Germany

²Carl von Ossietzky Universität Oldenburg, Institute of Physics, 26129 Oldenburg, Germany

(Dated: September 23, 2021)

Understanding the formation of lead halide (LH) perovskite solution precursors is crucial to gain insight into the evolution of these materials to thin films for solar cells. Using density-functional theory in conjunction with the polarizable continuum model, we investigate 18 complexes with chemical formula PbX_2M_4 , where $\text{X} = \text{Cl, Br, I}$ and M are common solvent molecules. Through the analysis of structural properties, binding energies, and charge distributions, we clarify the role of halogen species and solvent molecules in the formation of LH perovskite precursors. We find that interatomic distances are critically affected by the halogen species, while the energetic stability is driven by the solvent coordination to the backbones. Regardless of the solvent, lead iodide complexes are more strongly bound than the others. Based on the charge distribution analysis, we find that all solvent molecules bind covalently with the LH backbones and that Pb-I and Pb-Br bonds lose ionicity in solution. Our results contribute to clarify the physical properties of LH perovskite solution precursors and offer a valuable starting point for further investigations on their crystalline intermediates.

I. INTRODUCTION

Lead halide perovskites (LHPs) are among the most promising materials for the next generation of photovoltaic and opto-electronic applications [1–5]. One of their greatest advantages is their ability to be synthesized and processed in solution [6–10], thereby substantially reducing manufacturing costs for thin-film production [11–14]. The importance of solution chemistry in the synthesis and characterization of LHPs has stimulated dedicated research in the last few years [15–17]. Many studies have contributed to clarify the role of solvent-solute interactions in determining the crystal structure and the properties of the grown films [18–28]. An intricate interplay between solubility, polarity, dielectric screening, and coordinating ability has been accounted responsible for the efficacy of different solvents to form complexes with LHPs [20, 21, 29]. Furthermore, the choice of the solvent turned out to be a critical parameter for the formation of intermediate phases [19, 30–34] and even for the creation of defects in the final products [35, 36].

This vast body of experimental research has been supported by theoretical and computational work. The ability of *in silico* experiments to decouple the various effects in play has been exploited to interpret experimental data on the formation and the optical response of these systems [21, 37–40]. Additionally, high-throughput screening has been proven as a reliable and cost-effective method to explore large configurational spaces in view of the synthesis and characterization of these complex materials [21, 41].

Motivated by these successful contributions from theory, in this work, we want to further explore the formation of LHP solution precursors adopting a physicists' perspective. With state-of-the-art methods of *ab initio* electronic-structure theory, we investigate the stability,

the structural properties, and the charge distribution of charge-neutral LHP building blocks with chemical formula PbX_2 ($\text{X} = \text{Cl, Br, I}$) bound to four molecules of six common solvents (M), namely $\text{C}_2\text{H}_3\text{N}$ (ACN), $\text{C}_3\text{H}_7\text{NO}$ (DMF), $\text{C}_2\text{H}_6\text{OS}$ (DMSO), $\text{C}_4\text{H}_6\text{O}_2$ (GBL), $\text{C}_5\text{H}_9\text{NO}$ (NMP) and $\text{C}_4\text{H}_6\text{O}_3$ (PC) – see Figure 1. Although it is known that in experimental samples different lead halide species coexist [27, 37], we choose to focus on the aforementioned systems, which give rise to remarkable fingerprints in optical absorption measurements [27, 35, 42], to avoid accounting for additional electrostatic interactions with counterions to ensure charge neutrality. Our goal is to disclose general trends related to the energetics, the structural properties, and the charge distribution of PbX_2M_4 solvated compounds that are useful to gain further understanding on the solution chemistry of LHPs and also to interpret the formation of intermediate phases in their evolution to crystalline thin films. The approach adopted herein is complementary to computational-chemistry methods that are popular in the study of solution complexes, as well as to experiments in which these compounds are synthesized and characterized.

II. METHODOLOGY

The adopted *ab initio* formalism based on density-functional theory (DFT) [43–46] with the range-separated hybrid functional CAM-B3LYP [47] (see computational details in the Supporting Information) enables an accurate modeling and an insightful analysis of physical mechanisms in play. The representation of solute-solvent interactions through a hybrid atomistic/effective approach allows us to include both, the electronic interactions between PbX_2 and the nearest solvent molecules, as well as the dielectric screening induced to the lat-

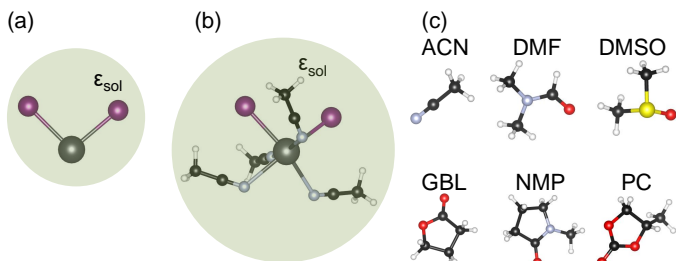


FIG. 1. a) Sketch of PbX_2 and b) PbX_2ACN_4 immersed in a solvent cavity; (c) Ball-and-stick representations of the solvent molecules considered in this work. Pb, I, O, S, C, H and N atoms are depicted in gray, purple, red, yellow, black, white and light blue, respectively.

ter in the liquid environment. In the considered structures, four solvent molecules are explicitly bound to the PbX_2 compounds, thereby resulting in charge-neutral complexes with chemical formula PbX_2M_4 ($\text{M} = \text{ACN}, \text{DMF}, \text{DMSO}, \text{GBL}, \text{NMP}, \text{and PC}$). These systems are embedded in a dielectric cavity described via the polarizable continuum model (PCM) [48] coupled to DFT, which accounts for the screening induced by the surrounding solvent molecules (Figure 1b). The following tabulated dielectric constants [49] are used to model the corresponding solvents: $\epsilon_{\text{DMSO}}=46.7$, $\epsilon_{\text{DMF}}=38.2$, $\epsilon_{\text{ACN}}=37.5$, $\epsilon_{\text{NMP}}=32.5$, $\epsilon_{\text{GBL}}=41.7$, $\epsilon_{\text{PC}}=64.0$. Isolated PbX_2 molecules in a solvent cavity with $\epsilon_{\text{ACN}}=37.5$ (see Figure 1a) are examined for comparison. We cross-checked these calculations using $\epsilon_{\text{PC}}=64.0$ and we noticed no change in the considered quantities.

We construct all 18 systems assuming an axial geometry of PbX_2 , which we found more stable in comparison with the equatorial X-Pb-X arrangement, in agreement with previous results on iodoplumbate compounds obtained at a similar level of theory [37]. By means of DFT calculations *in vacuo* [50–54], we checked that the enhanced stability of the compounds in the axial configuration is related to the more favorable charge distribution, which minimizes electron-electron repulsion between lead and halogen atoms (see Supporting Information, Figure S1 and Table S6, for further details). Four solvent molecules are explicitly attached to each PbX_2 backbone, thereby forming PbX_2M_4 complexes, which are optimized upon minimization of interatomic forces.

III. RESULTS AND DISCUSSION

The structural properties of the relaxed systems, summarized in Figure 2, are consistent with the intuition that the distance between the Pb atom and the halogen species critically depends on the size of the latter: the smaller the halogen atoms, the shorter their separation from Pb. The Pb-X distance is further enhanced by the presence of the explicit solvent molecules (Figure 2a). On

top of this, the dielectric screening of the implicit solvent cavity leads to a systematic and yet small increase of the Pb-X bond lengths on the order of 0.05 Å (see Supporting Information, Table S7), in agreement with previous findings on organic semiconductors in solution [55]. Bonding with DMSO leads to the most sizeable increments in the Pb-X bond lengths, consistent with the relatively large steric hindrance of this molecule. Likewise, the smallest changes with respect to the structure of PbX_2 are induced by the smallest considered moiety, ACN. In between, we find the trends induced by all the ringed compounds, such as GBL, NMP, and PC. The behavior of PbX_2DMF_4 is noteworthy. In the complexes containing Cl and Br, Pb-X distances are almost identical to those with GBL. On the other hand, Pb-I distances are enhanced by about 0.05 Å by the presence of Pb-DMF bonds, as a result of the steric hindrance of this solvent molecule enhanced by the large atomic radius of iodine. Our findings are in qualitative agreement with experimental reports of Pb-O distances in PbI_2 solvated in DMF and DMSO [56].

For PbI_2NMP_4 and PbI_2DMF_4 , we can compare the computed bond lengths with available experimental references [57, 58]. Our values for Pb-I and Pb-O distances (both NMP and DMF are bound to PbI_2 via O-bonds) agree well with the measurements [57, 58]. On average, our computed Pb-I bond lengths are consistent also with those measured for a crystalline phase of PbI_2 in DMF [30], whereby in the inorganic backbone the lead atoms are connected with five iodine neighbors. In that structure, however, Pb-O distances are approximately 0.1 Å lower compared to our estimates. On the other hand, Pb-I bond lengths detected in an intermediate phase of methylammonium lead iodine in DMF [59] are only a few hundreds of Å shorter than in our computational samples. This comparison suggests that the trends obtained in this study are relevant, at least qualitatively, also for the investigation of intermediate precursor phases of LHPs.

The variation of the X-Pb-X angle (see Figure 2b) is another indication of the non-trivial interplay between halogen species and solvent molecules in the final geometry of PbX_2M_4 . In the PbX_2 systems simulated in the implicit solvent cavity (see Figure 1a), the X-Pb-X angle exhibits a mild increase with the size of the halogen atoms. A similar trend but with systematically lower values is driven by the bonding of PbX_2 with the smallest considered solvent molecule, ACN. On the other hand, bonding to NMP leads to a steep increase of the X-Pb-X angle in all systems, especially in $\text{PbBr}_2\text{NMP}_4$ and in PbI_2NMP_4 , where variations with respect to the “bare” PbBr_2 and PbI_2 counterparts exceed 6° and 13°, respectively (see Supporting Information, Table S2). A monotonic enlargement of the X-Pb-X angle with increasing size of the halogen atom is also driven by PC, DMF, and GBL molecules. Bonding with PC leads to a sizeable reduction of the Cl-Pb-Cl angle compared to the isolated PbCl_2 , but to an insignificant variation in the compounds

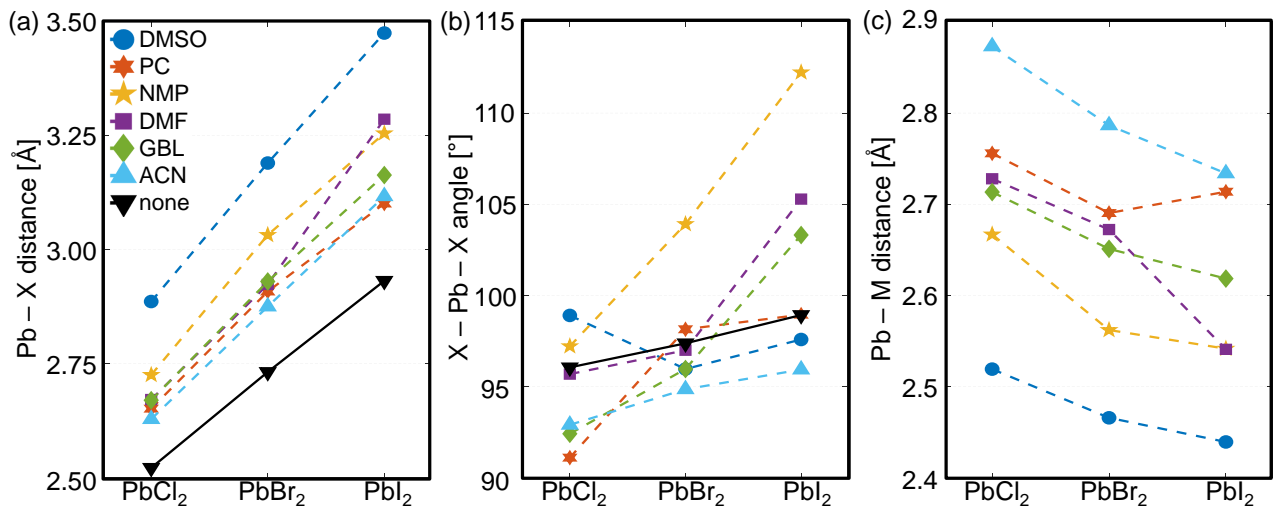


FIG. 2. Structural properties including (a) the average distance between lead and halogen atoms, (b) the angle of the PbX₂ backbone, and (c) the distance between lead atom and solvent molecule (M). For comparison, results for PbX₂ compounds without explicit solvent molecules (none) are reported in panels (a) and (b).

containing Br and I. Conversely, DMF does not cause any noticeable variation in the Cl-Pb-Cl and Br-Pb-Br angles, while enhancing the I-Pb-I angle by more than 5° (see Figure 2b). In the presence of GBL, the Cl-Pb-Cl angle is increased and the I-Pb-I angle is decreased, while the Br-Pb-Br one remains almost unaltered compared to PbBr₂. Finally, bonding with DMSO leads to an increment of Cl-Pb-Cl angle compared to PbCl₂ while to a reduction of the Br-Pb-Br and I-Pb-I angles. In this case, the dielectric screening of the solvent cavity leads to lower values compared than *in vacuo*, where the mutual interatomic repulsion is evidently larger (see Supporting Information, Tables S6 and S7).

Lastly, we analyze the average distance between the Pb atom and the solvent molecules in the considered complexes (see Figure 2c). With the exceptions of PC, in all examined systems this length decreases with increasing size of the halogen species. The solvent molecules are closest (furthest) from the central Pb atom in the presence of DMSO (ACN). It is worth noting that ACN is the only solvent that is bound to Pb via a N atom; all other molecules are connected through a Pb-O bond.

Next, we inspect the formation energies computed for all considered compounds in their optimized geometries analyzed above. The formation energy, E_f , is evaluated as

$$E_f = \frac{1}{4}(E_{tot} - E_{PbX_2} - E_{M_1} - E_{M_2} - E_{M_3} - E_{M_4}), \quad (1)$$

where E_{tot} is the total energy of the relaxed PbX₂M₄ system, and E_{PbX_2} and E_{M_i} are the energies of the building blocks in their geometry within the complex. With Eq. (1), we take into account separately the contribution of each individual solvent molecule in its own relaxed configuration, thereby accounting for variations among them

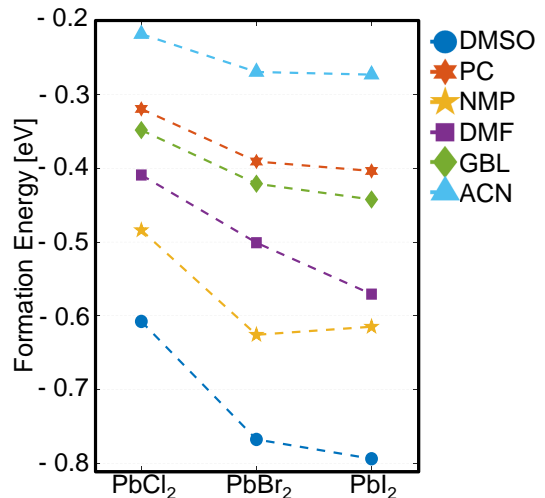


FIG. 3. Formation energies of all the considered compounds.

when bonded to the PbX₂ backbone. Stable complexes give rise to negative values of E_f : the more negative this quantity, the more stable the compound. Our results displayed in Figure 3 indicate that the most stable complexes are formed in the presence of DMSO, while the least stable ones include ACN. The general trend indicates higher stability at increasing size of the halogen species with the only exception of the complexes in NMP, where the interaction with PbBr₂ leads to a more negative formation energy. It is worth noting that the description of the systems in an implicit solvent cavity leads to a substantial enhancement of the formation energy compared to *in vacuo* conditions (see Table S7 in the Supporting Information).

The results for the formation energies reported in Figure 3 are consistent with the coordination ability of the

considered solvents in LHP solution precursors [31, 60], and are in line with previous theoretical predictions [21, 37]. A closer inspection of these data (see also Table S3 in the Supporting Information) reveals, however, a few differences. The values of formation energies reported in Ref. [37] are systematically larger than those summarized in Figure 3, with differences ranging from 0.05 to 0.10 eV that can be attributed to different computational parameters as well as to the slightly different formula adopted to estimate the formation energy. In Ref. [21], the bonding with PbX_2 is predicted to be more favorable with DMF rather than with NMP and, in general, values of formation energies are systematically larger than those calculated in the present work: this discrepancy can be again ascribed to the different approach for assessing the structural stability.

We conclude our analysis by inspecting the charge distribution within the simulated complexes. To do so, we make use of the Bader scheme [61–64], which enables a flexible partition of the charge density among different spatial domains. This method, based on the partition of the electron density computed from DFT is particularly useful in (hybrid) materials and interfaces formed by heterogeneous building blocks [65–69], and it is known to be more reliable than the Mulliken or the Hirshfeld schemes in systems with non-covalent bonds [70]. With the aim to understand the nature of the chemical bonds within the lead halide backbones as well as between them and the solvent molecules, we consider two types of partitions. First, we focus on the partial charges on Pb and on the halogen species in the PbX_2M_4 complexes (see Figure 4a-b). For comparison, PbX_2 in an implicit solvent cavity without solvent molecules attached is also considered. The results obtained for the latter systems confirm the net charge transfer between lead and halogen atoms and hence ionic nature of the Pb-X bond [71]. The trend shown in Figure 4b) indicates an increasingly negative charge in the less electronegative halogen atoms, with variations on the order of $0.1e^-$. This qualitative finding is in agreement with earlier experimental observations [72].

Examining now the results for the PbX_2M_4 complexes, we notice that the electronic interactions with the solvent molecules reduce the amount of negative charge on the heavier halogen species, thereby pointing to an enhancement of the covalent character of the Pb-I and Pb-Br bonds. This effect is less pronounced with DMSO which is the considered solvent molecule with the largest number of atoms, whereby the resulting charge distribution is more faceted. On the other hand, the character of the Pb-Cl bond is essentially unaltered by the interaction with the other solvent molecules, with the exceptions of DMSO and NMP.

The trends described above are reflected also in the total charge accumulated on the entire PbX_2 unit, computed as the sums of the partial charges on lead and halogen atoms (see Figure 4a-b) when interacting explicitly with the various solvent molecules (see Figure 4c).

In most systems, there is an almost perfect cancellation between the partial charges on the solvent molecules and those on the lead halide backbone. This cancellation is particularly efficient in presence of the electron-withdrawing solvents ACN, PC, and GBL. Based on these results, we conclude that covalent bonds are formed between Pb and the solvent molecules in almost all considered systems.

The only apparent deviation from this trend occurs with DMSO. Binding to this solvent molecule leaves the lead halide unit positively charged, with values between 0.1 and $0.2 e^-$ in presence of Cl and Br and above $0.4 e^-$ with iodine (see Table S4 in the Supporting Information). This result can be explained by considering the charge distribution occurring within DMSO. Already in the molecule, the oxygen lone pair generates a net charge close to $-2 e^-$ which is almost entirely compensated by the positive charge on the S atom. When DMSO is bound to PbX_2 , the charge on the O atom remains almost unaltered while the positive charge on S undergoes a decrease on the order of $0.2 e^-$ (see Table S5 in the Supporting Information). As a result, each DMSO molecule in $\text{PbX}_2\text{DMSO}_4$ carries a negative charge contribution that sums up to $-0.43 e^-$, leaving the same amount of charge with opposite sign on the lead halide backbone (see Figure 4c and Table S4).

We complement this analysis with the visual inspection of the total charge density on the PbX_2M_4 complexes, displayed in Figure 5. The largest contributions are visible on the solvent molecules and in particular on the ringed compounds DMF, GBL, and PC bound to PbCl_2 , and on NMP interacting with PbBr_2 . Depending on the solvent and halogen species, we can distinguish between systems where the charge is mainly spread across the solvent and others where it is primarily localized on specific atoms or groups. A clear trend is visible depending on the size of the halogen atom: The charge becomes more (less) localized in the systems bound to PC (DMSO and NMP). In the presence of DMF, GBL and ACN, variations among compounds with different backbones are much smaller. It is worth noting that in some cases, part of the charge is visible also on the halogen atoms, which is a signature of weaker charge transfer within the solvents. This is omnipresent in the considered compounds containing Cl, except when PC is involved. At the iso-values plotted in Figure 5, charge spills over onto Br only when PbBr_2 is bound to DMSO and ACN. Notably, no charge density appears on iodine atoms in PbI_2 -based compounds.

IV. SUMMARY AND CONCLUSIONS

In summary, we have presented a first-principles study of the formation of LHP solution precursors, focusing on charge-neutral systems with chemical formula PbX_2M_4 ($X = \text{Cl, Br, and I}$; $M = \text{DMSO, PC, NMP, DMF, GBL, and ACN}$). The analysis of the structural properties of

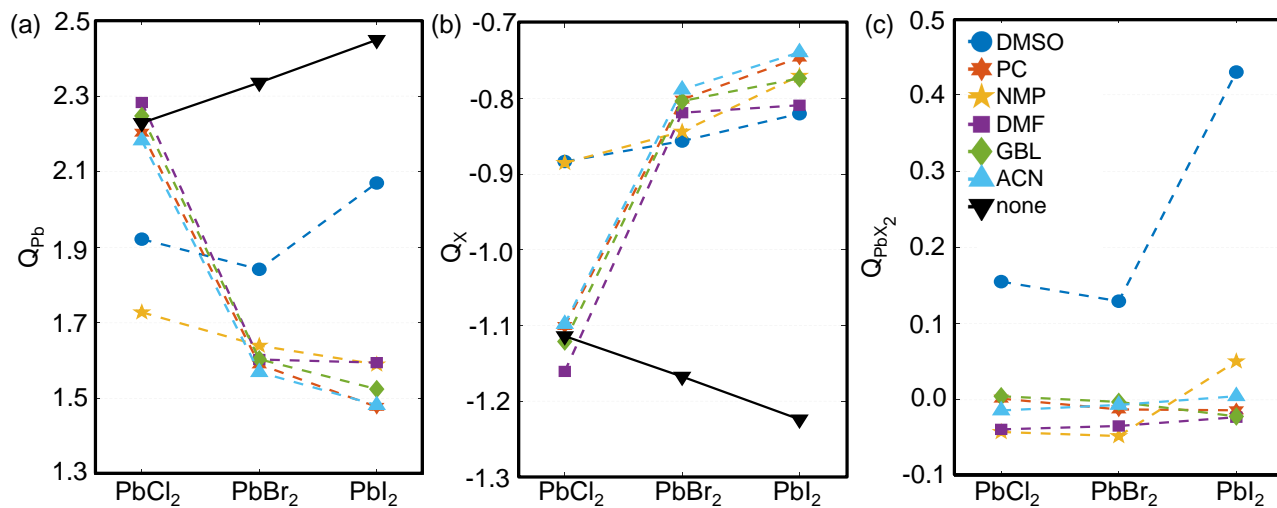


FIG. 4. Bader partial charges (a) on the Pb atom, (b) averaged on the halogen atoms, and (c) on the PbX_2 backbone. For comparison, results for PbX_2 without explicit solvent molecules (none) are reported in panels (a) and (b).

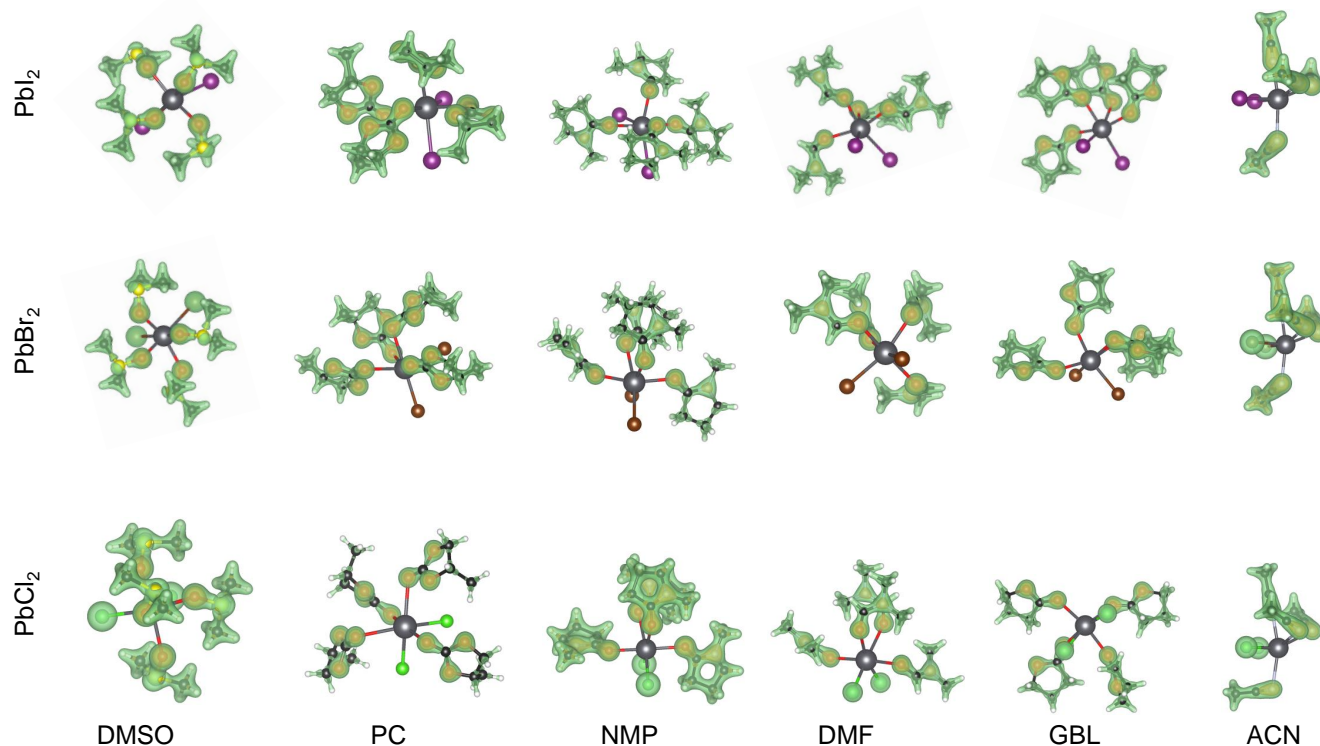


FIG. 5. Total electronic charge distribution on all the considered compounds depicted with two isosurfaces corresponding to 4% and 2% of the maximum value. Pb, I, O, S, C, H and N atoms are depicted in gray, purple, red, yellow, black, white, and light blue, respectively. Graphics prepared with the VESTA software [73].

the obtained complexes reveals how the steric hindrance of the solvent molecules affects bond lengths and angles of the PbX_2 backbone in the final geometries. Although the systems considered herein are only minimal units of actual LHP solution precursors, the general agreement of our computed bond lengths with those measured independently in various lead-iodide samples [30, 57–59], even in more advanced stages of the evolution of LHPs to thin films, make it reasonable to anticipate that the disclosed effects are relevant also in subsequent stages of crystallization of these materials. The computed formation energies confirm the anticipated trends based on the coordination ability of the various solvents: DMSO leads to the most stable structures while ACN to the least favorable ones, regardless of the halogen in the backbone. We also noticed a correlation between stability and size of the halogen species: Iodine-containing complexes are generally more stable than their counterparts with Cl or Br. Our analysis of the charge distribution, based on the Bader partition scheme, offers important indications on the nature of the chemical bonds and on the corresponding influence of the solvent molecules. The ionic character of the Pb-I and Pb-Br bonds is considerably mitigated by the interaction with all the considered solvents. On the other hand, the ionicity of the Pb-Cl remains unaltered except in presence of the electron-donating solvents DMSO and NMP, which tend to reduce it.

Our study, performed from the perspective and with state-of-the-art methods of electronic-structure theory, complements the extended body of chemical studies on the solution chemistry of LHPs. The presented quantum-mechanical analysis on the structural, energetic, and charge distribution properties of the considered compounds contributes to a deeper understanding of the fundamental properties of the solution precursors of these complex materials, shedding light on the nature and the strengths of their electronic stability and couplings. Our

results offer therefore a quantitative basis for future investigations on (pseudo)crystalline intermediate phases of LHPs in their evolution to thin-films for photovoltaic applications.

SUPPORTING INFORMATION

In the Supporting Information, we report the computational details, as well as additional information about the structural properties of the investigated compounds and the effects of the implicit solvents. The raw data plotted in Figure 2, Figure 3, Figure 4, and Figure 5 are also reported.

ACKNOWLEDGEMENTS

We are grateful to Giovanni Procida, Holger-Dietrich Saßnick, Oleksandra Shargaieva, and Eva Unger for fruitful discussions. This work was supported by the German Research Foundation (DFG), Priority Programm SPP 2196 - Project number 424394788, by the German Federal Ministry of Education and Research (Professorinnenprogramm III), and from the State of Lower Saxony (Professorinnen für Niedersachsen). A.C.R acknowledges financial support from the Erasmus+ Programme of the European Union. Calculations were performed on the HPC cluster CARL at the University of Oldenburg, funded by the DFG (project number INST 184/157-1 FUGG) and by the Ministry of Science and Culture of the Lower Saxony State.

DATA AVAILABILITY

The data that support the findings of this study are openly available in Zenodo at 10.5281/zenodo.4767389.

-
- [1] Ha ST, Liu X, Zhang Q, Giovanni D, Sum TC, Xiong Q. Synthesis of organic–inorganic lead halide perovskite nanoplatelets: towards high-performance perovskite solar cells and optoelectronic devices. *Adv. Optical Mater.* 2014; 2(9): 838–844.
- [2] Jeon NJ, Noh JH, Yang WS, et al. Compositional engineering of perovskite materials for high-performance solar cells. *Nature* 2015; 517(7535): 476–480.
- [3] Xiao Z, Kerner RA, Zhao L, et al. Efficient perovskite light-emitting diodes featuring nanometre-sized crystallites. *Nature Photon.* 2017; 11(2): 108–115.
- [4] Huang F, Li M, Siffalovic P, Cao G, Tian J. From scalable solution fabrication of perovskite films towards commercialization of solar cells. *Energy Environ. Sci.* 2019; 12(2): 518–549.
- [5] Andaji-Garmaroudi Z, Anaya M, Pearson AJ, Stranks SD. Photobrightening in lead halide perovskites: Observations, mechanisms, and future potential. *Adv. Energy Mater.* 2020; 10(13): 1903109.
- [6] Jeon NJ, Noh JH, Kim YC, Yang WS, Ryu S, Seok SI. Solvent engineering for high-performance inorganic–organic hybrid perovskite solar cells. *Nature Mat.* 2014; 13(9): 897–903.
- [7] Deschler F, Price M, Pathak S, et al. High photoluminescence efficiency and optically pumped lasing in solution-processed mixed halide perovskite semiconductors. *J. Phys. Chem. Lett.* 2014; 5(8): 1421–1426.
- [8] Zhao Y, Zhu K. Solution chemistry engineering toward high-efficiency perovskite solar cells. *J. Phys. Chem. Lett.* 2014; 5(23): 4175–4186.
- [9] Nie W, Tsai H, Asadpour R, et al. High-efficiency solution-processed perovskite solar cells with millimeter-scale grains. *Science* 2015; 347(6221): 522–525.
- [10] Cho H, Wolf C, Kim JS, et al. High-Efficiency Solution-Processed Inorganic Metal Halide Perovskite Light-Emitting Diodes. *Adv. Mater.* 2017; 29(31): 1700579.

- [11] Yi J, Zhuang J, Ma Z, et al. Regulated perovskite crystallinity via green mixed antisolvent for efficient perovskite solar cells. *Org. Electron.* 2019; 69: 69–76.
- [12] Ghosh S, Mishra S, Singh T. Antisolvents in Perovskite Solar Cells: Importance, Issues, and Alternatives. *Adv. Mater. Interfaces* 2020; 7(18): 2000950.
- [13] Zeng L, Chen S, Forberich K, Brabec CJ, Mai Y, Guo F. Controlling the crystallization dynamics of photovoltaic perovskite layers on larger-area coatings. *Energy Environ. Sci.* 2020; 13(12): 4666–4690.
- [14] Cui Y, Wang S, Ding L, Hao F. Green-Solvent-Processable Perovskite Solar Cells. *Adv. Energy Sustainability Res.* 2021; 2: 2000047.
- [15] McDowell C, Abdelsamie M, Toney MF, Bazan GC. Solvent additives: key morphology-directing agents for solution-processed organic solar cells. *Adv. Mater.* 2018; 30(33): 1707114.
- [16] Li B, Binks D, Cao G, Tian J. Engineering halide perovskite crystals through precursor chemistry. *Small* 2019; 15(47): 1903613.
- [17] Jung M, Ji SG, Kim G, Seok SI. Perovskite precursor solution chemistry: from fundamentals to photovoltaic applications. *Chem. Soc. Rev.* 2019; 48(7): 2011–2038.
- [18] Fu Y, Meng F, Rowley MB, et al. Solution growth of single crystal methylammonium lead halide perovskite nanostructures for optoelectronic and photovoltaic applications. *J. Am. Chem. Soc.* 2015; 137(17): 5810–5818.
- [19] Petrov AA, Sokolova IP, Belich NA, et al. Crystal structure of DMF-intermediate phases uncovers the link between CH₃NH₃PbI₃ morphology and precursor stoichiometry. *J. Phys. Chem. C* 2017; 121(38): 20739–20743.
- [20] Hamill Jr JC, Schwartz J, Loo YL. Influence of solvent coordination on hybrid organic-inorganic perovskite formation. *ACS Energy Lett.* 2017; 3(1): 92–97.
- [21] Stevenson J, Sorenson B, Subramaniam VH, et al. Mayer bond order as a metric of complexation effectiveness in lead halide perovskite solutions. *Chem. Mater.* 2017; 29(6): 2435–2444.
- [22] Foley BJ, Girard J, Sorenson BA, et al. Controlling nucleation, growth, and orientation of metal halide perovskite thin films with rationally selected additives. *J. Mater. Chem. A* 2017; 5(1): 113–123.
- [23] Fateev SA, Petrov AA, Khrustalev VN, et al. Solution processing of methylammonium lead iodide perovskite from γ -butyrolactone: crystallization mediated by solvation equilibrium. *Chem. Mater.* 2018; 30(15): 5237–5244.
- [24] Li Y, Zhi L, Ge G, et al. Investigation on Crystallization of CH₃NH₃PbI₃ Perovskite and Its Intermediate Phase from Polar Aprotic Solvents. *Cryst. Growth Des.* 2019; 19(2): 959–965.
- [25] Dutta A, Behera RK, Pradhan N. Solvent Polarity: How Does This Influence the Precursor Activation, Reaction Rate, Crystal Growth, and Doping in Perovskite Nanocrystals?. *ACS Energy Lett.* 2019; 4(4): 926–932.
- [26] Ortoll-Bloch AG, Herbol HC, Sorenson BA, Poloczek M, Estroff LA, Clancy P. Bypassing Solid-State Intermediates by Solvent Engineering the Crystallization Pathway in Hybrid Organic-Inorganic Perovskites. *Cryst. Growth Des.* 2019; 20(2): 1162–1171.
- [27] Shargaieva O, Näsström H, Smith JA, Többsens D, Munir R, Unger E. Hybrid perovskite crystallization from binary solvent mixtures: interplay of evaporation rate and binding strength of solvents. *Mater. Adv.* 2020; 1(9): 3314–3321.
- [28] More SA, Halor RG, Shaikh R, et al. Investigating the effect of solvent vapours on crystallinity, phase, and optical, morphological and structural properties of organolead halide perovskite films. *RSC Adv.* 2020; 10(66): 39995–40004.
- [29] Tutantsev AS, Udalova NN, Fateev SA, et al. New Pigeonholing Approach for Selection of Solvents Relevant to Lead Halide Perovskite Processing. *J. Phys. Chem. C* 2020; 124(20): 11117–11123.
- [30] Wakamiya A, Endo M, Sasamori T, et al. Reproducible fabrication of efficient perovskite-based solar cells: X-ray crystallographic studies on the formation of CH₃NH₃PbI₃ layers. *Chem. Lett.* 2014; 43(5): 711–713.
- [31] Li L, Chen Y, Liu Z, Chen Q, Wang X, Zhou H. The Additive Coordination Effect on Hybrids Perovskite Crystallization and High-Performance Solar Cell. *Adv. Mater.* 2016; 28(44): 9862–9868.
- [32] Jo Y, Oh KS, Kim M, et al. High performance of planar perovskite solar cells produced from PbI₂ (DMSO) and PbI₂ (NMP) complexes by intramolecular exchange. *Adv. Mater. Interfaces* 2016; 3(10): 1500768.
- [33] Cao J, Jing X, Yan J, et al. Identifying the molecular structures of intermediates for optimizing the fabrication of high-quality perovskite films. *J. Am. Chem. Soc.* 2016; 138(31): 9919–9926.
- [34] Vásquez-Montoya M, Montoya JF, Ramirez D, Jaramillo F. Understanding the precursor chemistry for one-step deposition of mixed cation perovskite solar cells by methylamine route. *J. Energy Chem.* 2021; 57: 386–391.
- [35] Rahimnejad S, Kovalenko A, Aranda C, Guerrero A. Coordination chemistry dictates the structural defects in lead halide perovskites. *Chem. Phys. Chem.* 2016; 17(18): 2795–2798.
- [36] Wang Y, Wu J, Zhang P, et al. Stitching triple cation perovskite by a mixed anti-solvent process for high performance perovskite solar cells. *Nano Energy* 2017; 39: 616–625.
- [37] Radicchi E, Mosconi E, Elisei F, Nunzi F, De Angelis F. Understanding the solution chemistry of lead halide perovskites precursors. *ACS Appl. Energy Mater.* 2019; 2(5): 3400–3409.
- [38] Radicchi E, Kachmar A, Mosconi E, Bizzarri B, Nunzi F, De Angelis F. Structural and Optical Properties of Solvated PbI₂ in γ -Butyrolactone: Insight into the Solution Chemistry of Lead Halide Perovskite Precursors. *J. Phys. Chem. Lett.* 2020; 11(15): 6139–6145.
- [39] Radicchi E, Ambrosio F, Mosconi E, Alasmari AA, Alasmari FA, De Angelis F. Combined Computational and Experimental Investigation on the Nature of Hydrated Iodoplumbate Complexes: Insights into the Dual Role of Water in Perovskite Precursor Solutions. *J. Phys. Chem. B* 2020; 124(50): 11481–11490.
- [40] Valencia AM, Shargaieva O, Schier R, Unger E, Cocchi C. Optical Fingerprints of Polynuclear Complexes in Lead Halide Perovskite Precursor Solutions. *J. Phys. Chem. Lett.* 2021; 12: 2299–2305.
- [41] Gu E, Tang X, Langner S, et al. Robot-Based High-Throughput Screening of Antisolvents for Lead Halide Perovskites. *Joule* 2020; 4(8): 1806–1822.
- [42] Shargaieva O, Kuske L, Rappich J, Unger E, Nickel NH. Building blocks of hybrid perovskites: A photoluminescence study of lead-iodide solution species.

- Chem. Phys. Chem.* 2020; 21(20): 2327.
- [43] Hohenberg P, Kohn W. Inhomogeneous Electron Gas. *Phys. Rev.* 1964; 136: B864–B871.
- [44] Kohn W, Sham LJ. Self-Consistent Equations Including Exchange and Correlation Effects. *Phys. Rev.* 1965; 140: A1133–A1138.
- [45] Frisch MJ, Trucks GW, Schlegel HB, et al. Gaussian 16 Revision A.03. 2016. Gaussian Inc. Wallingford CT.
- [46] Grimme S, Antony J, Ehrlich S, Krieg H. A consistent and accurate ab initio parametrization of density functional dispersion correction (DFT-D) for the 94 elements H–Pu. *J. Chem. Phys.* 2010; 132(15): 154104.
- [47] Yanai T, Tew DP, Handy NC. A new hybrid exchange–correlation functional using the Coulomb-attenuating method (CAM-B3LYP). *Chem. Phys. Lett.* 2004; 393(1): 51–57.
- [48] Tomasi J, Mennucci B, Cammi R. Quantum mechanical continuum solvation models. *Chem. Rev.* 2005; 105(8): 2999–3094.
- [49] Wohlfarth C. Static Dielectric Constants of Pure Liquids and Binary Liquid Mixtures: Supplement to Volume IV/17 (Landolt–Börnstein: Numerical Data and Functional Relationships in Science and Technology–New Series). 2015.
- [50] Blum V, Gehrke R, Hanke F, et al. Ab Initio Molecular Simulations with Numeric Atom-Centered Orbitals. *Comput. Phys. Commun.* 2009; 180: 2175–2196.
- [51] Havu V, Blum V, Havu P, Scheffler M. Efficient O(N) Integration for All-Electron Electronic Structure Calculation Using Numeric Basis Functions. *J. Comp. Phys.* 2009; 228(22): 8367–8379. doi: <https://doi.org/10.1016/j.jcp.2009.08.008>
- [52] Perdew JP, Burke K, Ernzerhof M. Generalized Gradient Approximation Made Simple. *Phys. Rev. Lett.* 1996; 77: 3865–3868.
- [53] Tkatchenko A, Scheffler M. Accurate Molecular Van Der Waals Interactions from Ground-State Electron Density and Free-Atom Reference Data. *Phys. Rev. Lett.* 2009; 102: 073005.
- [54] Hirshfeld FL. Bonded-Atom Fragments for Describing Molecular Charge Densities. *Theor. Chem. Acta* 1977; 44(2): 129–138.
- [55] Krumland J, Valencia AM, Cocchi C. Exploring organic semiconductors in solution: the effects of solvation, alkylation, and doping. *Phys. Chem. Chem. Phys.* 2021; 23(8): 4841–4855.
- [56] Wu Y, Islam A, Yang X, et al. Retarding the crystallization of PbI₂ for highly reproducible planar-structured perovskite solar cells via sequential deposition. *Energy Environ. Sci.* 2014; 7(9): 2934–2938.
- [57] Sharenko A, Mackeen C, Jewell L, Bridges F, Toney MF. Evolution of iodoplumbate complexes in methylammonium lead iodide perovskite precursor solutions. *Chem. Mater.* 2017; 29(3): 1315–1320.
- [58] Hamill Jr JC, Romiluyi O, Thomas SA, et al. Sulfur-donor solvents strongly coordinate Pb²⁺ in hybrid organic–inorganic perovskite precursor solutions. *J. Phys. Chem. C* 2020; 124(27): 14496–14502.
- [59] Hao F, Stoumpos CC, Liu Z, Chang RP, Kanatzidis MG. Controllable perovskite crystallization at a gas–solid interface for hole conductor-free solar cells with steady power conversion efficiency over 10%. *J. Am. Chem. Soc.* 2014; 136(46): 16411–16419.
- [60] Li W, Fan J, Li J, Mai Y, Wang L. Controllable grain morphology of perovskite absorber film by molecular self-assembly toward efficient solar cell exceeding 17%. *J. Am. Chem. Soc.* 2015; 137(32): 10399–10405.
- [61] Bader RFW. *Atoms in Molecules - A Quantum Theory*. Atoms in Molecules: a Quantum Theory. Oxford University Press, Oxford, UK . 1990.
- [62] Henkelman G, Arnaldsson A, Jónsson H. A fast and robust algorithm for Bader decomposition of charge density. *Comp. Mater. Sci.* 2006; 36(3): 354–360.
- [63] Sanville E, Kenny SD, Smith R, Henkelman G. Improved grid-based algorithm for Bader charge allocation. *J. Comput. Chem.* 2007; 28(5): 899–908.
- [64] Tang W, Sanville E, Henkelman G. A grid-based Bader analysis algorithm without lattice bias. *J. Phys. Condens. Matter.* 2009; 21(8): 084204.
- [65] Niu S, Liu S, Liu B, et al. High energetic polymeric nitrogen sheet confined in a graphene matrix. *RSC Adv.* 2018; 8(54): 30912–30918.
- [66] Marchal N, Van Gompel W, Gelvez-Rueda MC, et al. Lead-Halide Perovskites Meet Donor–Acceptor Charge-Transfer Complexes. *Chem. Mater.* 2019; 31(17): 6880–6888.
- [67] Valencia AM, Guerrini M, Cocchi C. Ab initio modelling of local interfaces in doped organic semiconductors. *Phys. Chem. Chem. Phys.* 2020; 22(6): 3527–3538.
- [68] Jacobs M, Krumland J, Valencia AM, Wang H, Rossi M, Cocchi C. Ultrafast charge transfer and vibronic coupling in a laser-excited hybrid inorganic/organic interface. *Adv. Phys. X* 2020; 5(1): 1749883.
- [69] Schier R, Valencia AM, Cocchi C. Microscopic Insight into the Electronic Structure of BCF-Doped Oligothiophenes from Ab Initio Many-Body Theory. *J. Phys. Chem. C* 2020; 124(26): 14363–14370.
- [70] Saha S, Roy RK, Ayers PW. Are the Hirshfeld and Mulliken population analysis schemes consistent with chemical intuition?. *Int. J. Quantum Chem.* 2009; 109(9): 1790–1806.
- [71] Borghesi C, Radicchi E, Belpassi L, Meggiolaro D, De Angelis F, Nunzi F. The nature of the lead-iodine bond in PbI₂: A case study for the modelling of lead halide perovskites. *Comp. Theo. Chem.* 2019; 1164: 112558.
- [72] Bengtsson L, Holmberg B. Cationic lead (II) halide complexes in molten alkali-metal nitrate. Part 2.—A thermodynamic investigation of the chloride, bromide and iodide systems. *J. Chem. Soc., Faraday Trans.* 1989; 85(2): 317–329.
- [73] Momma K, Izumi F. VESTA 3 for three-dimensional visualization of crystal, volumetric and morphology data. *J. Appl. Cryst.* 2011; 44(6): 1272–1276.